Vortex nucleation processes in rotating lattices of Bose-Einstein condensates ruled by the on-site phases

D. M. Jezek[1,*] and P. Capuzzi [2,1]

[1]*CONICET - Universidad de Buenos Aires, Instituto de Física de Buenos Aires (IFIBA), Ciudad Universitaria, 1428 Buenos Aires, Argentina*
[2]*Universidad de Buenos Aires, Facultad de Ciencias Exactas y Naturales, Departamento de Física, Ciudad Universitaria, 1428 Buenos Aires, Argentina*

We study the nucleation and dynamics of vortices in rotating lattice potentials where weakly linked condensates are formed with each condensate exhibiting an almost axial symmetry. Due to such a symmetry, the on-site phases acquire a linear dependence on the coordinates as a result of the rotation, which allows us to predict the position of vortices along the low-density paths that separate the sites. We first show that, for a system of atoms loaded in a four-site square lattice potential, subject to a constant rotation frequency, the analytical expression that we obtain for the positions of vortices of the stationary arrays accurately reproduces the full three-dimensional Gross-Pitaevskii results. We then study the time-dependent vortex nucleation process when a linear ramp of the rotation frequency is applied to a lattice with 16 sites. We develop a formula for the number of nucleated vortices which turns out to have a linear dependence on the rotation frequency with a smaller slope than that of the standard estimate which is valid in the absence of the lattice. From time-dependent Gross-Pitaevskii simulations we further find that the on-site populations remain almost constant during the time evolution instead of spreading outwards, as expected from the action of the centrifugal force. Therefore, the time-dependent phase difference between neighboring sites acquires a running behavior typical of a self-trapping regime. We finally show that, in accordance with our predictions, this fast phase-difference evolution provokes a rapid vortex motion inside the lattice. Our analytical expressions may be useful for describing other vortex processes in systems with the same on-site axial symmetry.

I. INTRODUCTION

In the past decades the study of the dynamics of quantized vortices in superfluid systems [1] has been an active area of research. In confined Bose-Einstein condensates (BECs) [2] the first experimental realization that succeeded in generating and observing a vortex was performed in 1999 [3], and subsequently Anderson *et al.* measured the precession frequency of a vortex moving around the axis of a harmonic trapping potential [4]. Such experiments have constituted the starting point of a growing number of works on either static or dynamical configurations of vortices in BECs within different types of confining potentials (see [5] and references therein). Among them, the most commonly used trapping potentials are the harmonic, quadratic plus quartic, and toroidal ones, to which optical lattices may also be superimposed. The low-density regions of such condensates, such as the central hollow of a torus, have shown to favor the pinning of vortices, whereas, for rotating systems with superimposed optical lattices, the low-density paths that connect the outside and inside of the condensate help to reduce the vortex nucleation frequency. The reason is that the energy barrier for a vortex to enter the system becomes flattened when lowering such density.

The first experiments on producing arrays of many vortices were performed with rotating harmonic traps for large enough

rotation frequencies [6–8] and rotating quadratic plus quartic potentials for even larger frequencies [9,10]. Then experiments dealing on quantized circulation have included toroidal trapping potentials [11–13]. In the more recent realization [13], a multiply quantized superfluid circulation has been generated about the central density hollow with a winding number around the torus as high as 11, which persisted for at least 3 s. From the theoretical point of view, in such toroidal trappings, stationary arrays of vortices have been studied in rotating systems [14,15] and in nonrotating ones [16,17]. Finally, in rotating optical lattices, some pioneer theoretical studies in searching equilibrium vortex configurations have been carried out [18–20]. Such works dealt with vortices that became pinned on the density minima, which was latterly experimentally observed by Tung *et al.* [21] in triangular and square lattices, whereas for sufficient rotation intensity they reported a structural crossover to a vortex lattice. From then on, these studies were extended to include other systems, e.g., mixtures of species with more complex types of atomic interactions, such as the dipolar one [22]. More recently, researchers have also analyzed the consequences of including finite temperature effects [23].

In an experimental work in a rotating lattice [24], the vortex nucleation process has been undertaken in a rather distinct manner, since the optical lattice was subject to a time-varying rotation frequency. In such work it has been observed that the number of nucleated vortices increased linearly as a function of the frequency for barriers high enough so that the system can be considered as formed by weakly linked condensates

---

*Corresponding author: djezek@df.uba.ar

(WLCs). In the present work, although we use a simpler system, we work with WLCs and apply similar dynamical conditions to those of the experiment, with the aim to better understand such vortex nucleation process. An early attempt to theoretically describe such results [25] includes an *ad hoc* dissipation parameter to relax the system into the equilibrium configuration, although in view of some mismatches that appear with respect to the experimental data, it might not be the experimental case.

It is interesting to mention that density profiles similar to those of lattice systems can be attained in the supersolid phase of dipolar BECs [26–28] given that the formed particle droplets are separated by low-density valleys. Hence, in rotating condensates the nucleation of vortices become more favored in the supersolid phase than in the superfluid one. In particular, it was shown that low-density regions tend to reduce the energetic barrier for a vortex to enter the system, and thus lower the nucleation frequency and help in pinning vortices in the interstitial zones between droplets [27]. We finally note that in an experimental work, vortices have been recently observed in dipolar condensates [29].

The goal of this work consists in showing that for WLCs formed in deep lattice potentials, the expressions for the rotation-induced on-site phases constitute a powerful tool for describing the nucleation and dynamics of vortices. In Ref. [30] it has been observed that when a ring-shaped lattice is subject to rotation, the induced on-site phase of each localized function (LF), and hence the associated velocity field, depends on the geometry of the corresponding well. In some cases, such LF phases acquire a simple expression, with a linear dependence on the coordinates. In this work we will obtain an analytical formula for predicting the position of vortices on rotating optical lattices by using such phases' expressions. The formalism applies to square lattices for which the system can be considered to be formed by WLCs with each of the condensates having an approximately axial symmetry around a direction parallel to the rotation axis. In particular, we will focus our study on four- and 16-site square lattices confined by a harmonic potential. For the four-site system the LFs are obtained by a basis transformation from four Gross-Pitaevskii (GP) stationary states. Considering that the order parameter can be written as a linear combination of the on-site LFs with their corresponding phases, the location of vortices is determined by searching the zeros of such an order parameter. The vortex positions between two neighboring sites can be easily obtained by considering only both associated LFs. In doing so we obtain the stationary array of vortices in the case of a lattice of four sites, which show to be in very good accordance with the vortex positions obtained by GP simulations. In a second step, we generalize such a formula for a lattice which does not exhibit a ring-type form, and hence the LFs cannot be obtained through a basis transformation. Nevertheless, in order to find the vortex positions, due to the sites' symmetry, we can assume that the LFs phases acquire the same analytic expressions. Finally, we analyze the vortex nucleation process when the rotation frequency varies linearly in time from zero to the radial trap frequency, reproducing the dynamical conditions applied in the experimental device [24]. Although we do not adjust the size of the lattice and parameters to the experimental ones, the present study allows

us to analyze the dynamical characteristics of a similar time-dependent nucleation process.

The paper is organized as follows. In Sec. II we describe the theoretical framework for the four-site ring-shaped lattice and analyze the spatial validity range of the phase expression for the on-site localized function described in Ref. [30]. In Sec. III we obtain the stationary arrays of vortices for the rotating ring-shaped lattice at two given frequencies, whereas in Sec. IV we study the vortex nucleation process when applying a time-linear ramp of the rotation frequency for a 16-site square lattice. In particular, we determine the number of nucleated vortices as a function of the rotation frequency and analyze the involved vortex dynamics during such a process. Finally, Sec. VI is devoted to our conclusions.

II. THEORETICAL FRAMEWORK

A. On-site localized functions for a ring-shaped lattice

Given we consider high barriers between sites, a quite accurate approximation of the order parameter is obtained by a superposition of on-site LFs. A previous work described the method for obtaining such localized states for a rotating ring-shaped lattice system [30]. Summarizing, one should first obtain the stationary states $\psi_n(\mathbf{r})$ by solving the corresponding GP equation [31],

$$[\hat{H}_0 + gN|\psi_n(\mathbf{r})|^2 - \mathbf{\Omega} \cdot \hat{L}]\psi_n(\mathbf{r}) = \mu_n\psi_n(\mathbf{r}), \quad (1)$$

where $\hat{H}_0 = -\frac{\hbar^2}{2m}\nabla^2 + V_t$ with V_t the trapping potential, $g = 4\pi a\hbar^2/m$ is the 3D coupling constant in terms of the *s*-wave scattering length a of the atoms, $\hat{L}$ is the angular momentum operator, and $\mathbf{\Omega} = \Omega\hat{z}$ is the applied angular rotation frequency around the z axis. For a nonrotating system, the index n denotes the winding number, where the velocity field circulation is calculated along a circle that passes by the links around the lattice. Such a winding number is generated through a phase-imprinting method performed on the order parameter before the minimization procedure. For a number of sites N_s, the possible independent states are restricted to values of n in the interval $-||(N_s - 1)/2|| \leqslant n \leqslant ||N_s/2||$ [32], where $||.||$ denotes the standard integer part, whereas in a rotating system, using the same phase-imprinting method, depending on the value of Ω, the winding number of the outcome of the minimization can change in N_s units. Hence, the different stationary order parameters can still be labeled with the same values of n, restricted to $-||(N_s - 1)/2|| \leqslant n \leqslant ||N_s/2||$ [30], although n may not correspond to the actual winding number. It has been shown in Ref. [32] that the stationary states with different n values are orthogonal. Furthermore, one can define a set of N_s orthonormal LFs, given by the following basis transformation [30]:

$$w_k(\mathbf{r}) = \frac{1}{\sqrt{N_s}} \sum_n \psi_n(\mathbf{r}) e^{-in\theta_k}, \quad (2)$$

where $\theta_k = 2\pi k/N_s$. The index k labels the site where the function is localized. For $N_s = 4$, the value $k = 0$ corresponds to the quadrant $x > 0$ and $y > 0$, and k increases in the counterclockwise direction around the ring from $k = -1$ to $k = 2$. It is important to note that the choice of the global phase of each $\psi_n(\mathbf{r})$ can affect the localization of the LFs. A discussion

of how to choose such a phase in order to achieve maximum localization is given in [33]. In this work we set $\arg(\psi_n(\mathbf{r}))=0$ at the bisector of the $k = 0$ site. We note that, in contrast to the nonrotating case, the on-site LF obtained through Eq. (2), cannot be reduced to a real function. Due to the rotation, the wave functions $\psi_n(\mathbf{r})$ have a nonvanishing velocity field within each site and hence carry a spatially inhomogeneous phase profile. This inhomogeneity in the on-site phase is then transferred to the LFs through Eq. (2).

Finally, the order parameter can be approximated employing the LFs as

$$\psi(\mathbf{r}, t) = \sum_k b_k(t) \, w_k(\mathbf{r}), \tag{3}$$

with $b_k(t) = \sqrt{n_k(t)}e^{i\phi_k(t)}$, where $n_k = N_k/N$ with N_k the occupation number at the site k. We note that the global time-dependent phase $\phi_k(t)$ does not represent the actual phase in the k-site when $\Omega \neq 0$, but it takes into account only its time dependence, while as we have mentioned the spatial profile of the phase is carried out by the complex function $w_k(\mathbf{r})$.

B. The system

The condensate is formed by rubidium atoms and the trapping potential is given by

$$V_t(\mathbf{r}) = \tfrac{1}{2}m\big[\omega_r^2 r^2 + \omega_z^2 z^2\big] + V_b[\cos^2(\pi x/d) + \cos^2(\pi y/d)], \tag{4}$$

where $r^2 = x^2 + y^2$ and m is the atom mass. Hereafter, the time, energy, and length will be given in units of ω_r^{-1}, $\hbar\omega_r$, and $l_r = \sqrt{\hbar/(m\omega_r)}$, respectively.

For the four-site, ring-shaped lattice we have chosen the harmonic frequencies $\omega_r = 2\pi \times 70$ Hz and $\omega_z = 2\pi \times 90$ Hz, and the intersite distance $d = 3.9l_r = 5.1\,\mu$m. The barrier height of the lattice is fixed at $V_b = 25\hbar\omega_r$ in order to obtain a system of four WLCs for a number of particles of $N = 10^4$ [30].

C. Validity range for the expression of the rotation induced on-site phases

When the ring-shaped lattice is subject to rotation, the LF phases acquire a linear dependence on the x and y coordinates, related to a homogeneous velocity field [30]. Such a velocity field profile is a consequence of the almost axial symmetry of each localized on-site density around an axis parallel to the z direction. In Ref. [30], an analytical expression for the phase on each site has been obtained. In this section we will show that such an expression is valid in a wide region that includes the straight segments that separates the sites.

In particular, it has been shown [30] that the LF for the k-site can be written as

$$w_k(\mathbf{r}, \Omega) = |w_k(\mathbf{r}, \Omega)|e^{i\frac{m}{\hbar}(\mathbf{r}-\mathbf{r}_{cm}^k)\cdot(\mathbf{\Omega}\times\mathbf{r}_{cm}^k)}, \tag{5}$$

where $\mathbf{r}_{cm}^k$ is the center of mass of the localized density $|w_k(\mathbf{r}, \Omega)|^2$. Hereafter, for simplicity, we will omit writing the implicit LF dependence on Ω.

Such a particular phase dependence on the coordinates has important consequences on the vortex nucleation phenomenon, which takes place along low-density paths that
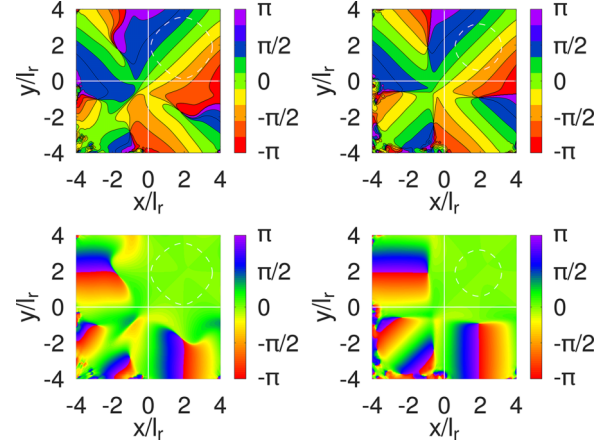

FIG. 1. Top panels: Phase of $w_0(x, y, z_i)$ from Eq. (2) for $\Omega/2\pi = 28$ Hz, at the planes $z_1 = 0$ and $z_2 = 3l_r$ in the left and right panels, respectively. The form of the phase around the other sites is necessary to ensure $w_0(x, y, z_i) \perp w_k(x, y, z_i)$, with $k \neq 0$. Bottom panels: Phase of $w_0(x, y, z_i)\,e^{-iA(-x+y)}$ for the same Ω and z planes of the top panels. The dashed lines indicate the isodensity contour of such a LF with a value of 10^{-3} of the maximum density. The color scales correspond to $\arg(w_0(\mathbf{r}))$ and $\arg(w_0(\mathbf{r})\,e^{-iA(-x+y)})$ in the top and bottom panels, respectively.

connect the lattice junctions. Due to the discrete symmetry, we will concentrate ourselves on a specific junction, but the results remain valid for the other ones. In particular, we consider the junction that separates the $k = 0$ and $k = 1$ sites, which lies along the semiaxis $y > 0$. We first rewrite Eq. (5) in terms of the center-of-mass coordinates: $\mathbf{r}_{cm}^k = (x_k, y_k, 0)$ as

$$w_k(\mathbf{r}) = |w_k(\mathbf{r})|e^{i\frac{m}{\hbar}(yx_k - xy_k)\Omega}. \tag{6}$$

For the trapping potential here considered, the coordinates of the center of mass of the localized densities verify $x_1 = -x_0$ and $y_1 = y_0$, and their absolute values may be taken equal to $d/2$. Then the neighboring LFs read

$$w_0(x, y, z) = |w_0(\mathbf{r})| \, e^{iA(-x+y)}, \tag{7}$$

$$w_1(x, y, z) = |w_1(\mathbf{r})| \, e^{-iA(x+y)}, \tag{8}$$

where $A = dm\Omega/(2\hbar)$.

In the top panel of Fig. 1 we show the LF phase profile for the $k = 0$ site, given by Eq. (2), at the $z = 0$ and $z = 3l_r$ planes, in the left and right panels, respectively. In such panels it may be seen that the LF has a phase gradient with the shape of Eq. (7) within the site. Moreover, in the bottom panels we depict such a phase minus its approximate analytic expression of Eq. (7). It may be seen that the resulting phase turns out to be zero around the region determined by $x > 0$ and $y > 0$, for both z planes. We further note that given that the area of homogeneity is slightly larger than the mentioned quadrant, the actual phase $A(-x + y)$ remains valid surpassing the neighborhood of the junctions. Then one can safely use the order parameter of the type of Eq. (3), with the expression for the LFs given by Eq. (5), along the low-density paths that separate the sites. As we will see, such an expression with the analytical phase turns out to be crucial to correctly define the location of vortices.

III. VORTEX NUCLEATION ON STATIONARY STATES IN A RING-SHAPED LATTICE

A. Vortex nucleation on $\psi_0(\mathbf{r})$

In order to analyze the appearance of vortices in the simplest case, and in view that in current experiments the system is initially in a vortex free state, we will first focus on the $n = 0$ stationary order parameter. For a fixed Ω value such a state, in terms of the LFs, with the on-site velocity field provided by the rotation, is given by

$$\psi_0(\mathbf{r}) = \frac{1}{\sqrt{N_s}} \sum_k w_k(\mathbf{r}). \qquad (9)$$

It is well known that a superfluid system is characterized by an irrotational flow given by the condition on the velocity field $\nabla \times \mathbf{v}(\mathbf{r}) = 0$. Since the vortex has a nonvanishing velocity field circulation around its core, it implies that the density should vanish at the coordinates of the vortex line $\mathbf{R}_v = (X_v, Y_v, z)$ to guarantee the superfluid condition in every point of the fluid. Hence, we will analytically obtain such coordinates of the vortex for the junction around $x \simeq 0$ with $y > 0$, by searching the points that verify $\psi_0(\mathbf{R}_v) = 0$, which yields a vanishing density.

Using the analytic expression for the phases of the LFs and retaining only the terms of the order parameter that include the relevant localized states around that junction, we obtain the vortex position by solving $\sqrt{N_s}\psi_0(\mathbf{R}_v) = w_0(\mathbf{R}_v) + w_1(\mathbf{R}_v) = 0$ with the approximations of Eqs. (7) and (8). This yields the following equation:

$$|w_0(\mathbf{R}_v)| e^{iA(-X_v+Y_v)} + |w_1(\mathbf{R}_v)| e^{-iA(X_v+Y_v)} = 0, \qquad (10)$$

which can be rewritten as

$$e^{-iA(X_v+Y_v)}(|w_0(\mathbf{R}_v)| e^{i2AY_v} + |w_1(\mathbf{R}_v)|) = 0. \qquad (11)$$

Taking into account the real and imaginary parts of the previous equation we further obtain

$$|w_0(\mathbf{R}_v)| \cos(2AY_v) + |w_1(\mathbf{R}_v)| = 0 \qquad (12)$$

and

$$\sin(2AY_v) = 0, \qquad (13)$$

respectively.

Equation (13) implies $2AY_v = \pi k'$, where k' is a natural number, whereas Eq. (12) restricts such a value to an odd number $k' = 2l + 1$ given that it should verify $\cos(\pi k) = -|w_1(X_v, Y_v, z)|/|w_0(X_v, Y_v, z)| = -1$. We note that the condition for the absolute values of the localized states, taking into account the symmetry, is fulfilled for $X_v = 0$, whereas from the other conditions, one obtains the expression for the Y_v coordinate along the low-density path between the $k = 0$ and the $k = 1$ sites,

$$Y_v(l) = (2l + 1)\frac{\pi\hbar}{md\Omega}, \qquad (14)$$

where $l \geqslant 0$ labels the sequence of vortices that enter the system from the $y > 0$ border of the lattice. Moreover, given the fourfold symmetry of the lattice, each l value defines the positions of four vortex lines: $(0, Y_v(l), z)$, $(Y_v(l), 0, z)$, $(0, -Y_v(l), z)$, and $(-Y_v(l), 0, z)$, in the whole system.
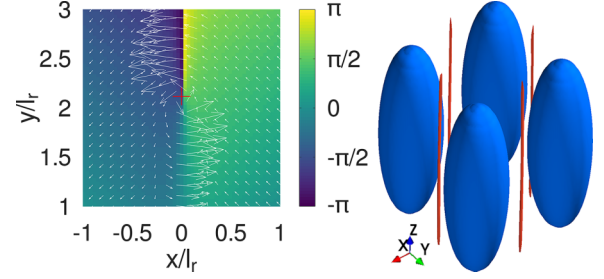

FIG. 2. Left panel: Phase (in colors) and velocity field (arrows) extracted from the GP order parameter $\psi_0(\mathbf{r})$ around the junction $y > 0$ and at the $z = 0$-plane for $\Omega/(2\pi) = 28$ Hz. The position of the vortex, obtained by the plaquette method, is marked with a red plus sign. Right panel: Three-dimensional configuration of the on-site condensates (blue) and the vortex lines (red) extracted from GP simulations. The color scale in the left panel corresponds to arg $(\psi_0(\mathbf{r}))$. The border of the condensate in the right panel is fixed at a density of 5×10^{-2} of its maximum value.

In the left panel of Fig. 2 we show with colors the phase and the corresponding velocity field of $\psi_0(\mathbf{r})$ obtained from the GP (1), for the rotation frequency $\Omega/(2\pi) = 28$ Hz. There we mark with a red plus sign a vortex position which has been extracted from such a state using the plaquette method of Ref. [34]. It may be seen that for $l = 0$, the estimate given by Eq. (14) yields $Y_v(0) = 2.03l_r$, which is in good accordance with the GP result. Such a position corresponds to a point of the vortex line $(0, Y_v(0), z)$. In the right panel we show the full system in three dimensions, with the four vortex lines. We note that such vortices coincide with straight lines parallel to the z axis as we have stated.

B. Vortex nucleation on the stationary states

We now extend the study to stationary states with arbitrary n values. It is interesting to note that such states change their relative energy values when varying the rotation frequency [30], hence the ground state is not achieved at a fixed n value for any Ω. By inverting the basis transformation of Eq. (2), such stationary states in terms of the LFs acquire the form

$$\psi_n(\mathbf{r}) = \frac{1}{\sqrt{N_s}} \sum_k w_k(\mathbf{r}) e^{ink2\pi/N_s} \qquad (15)$$

for $n \in \{-1, 0, 1, 2\}$. In an analogous manner to the described in the previous subsection, we can obtain the Y_v coordinate for the junction between $k = 0$ and $k = 1$ sites. We then search the solution of

$$|w_0(\mathbf{R}_v)| e^{iA(-X_v+Y_v)} + |w_1(\mathbf{R}_v)| e^{-iA(X_v+Y_v)+i2\pi n/N_s} = 0, \qquad (16)$$

where $\mathbf{R}_v = (X_v, Y_v, z)$, from which the following equation should hold:

$$|w_0(\mathbf{R}_v)| e^{i(2AY_v - 2\pi \frac{n}{N_s})} + |w_1(\mathbf{R}_v)| = 0, \qquad (17)$$

which is satisfied by $2AY_v - 2\pi n/N_s = \pi(2l + 1)$. Therefore, using that $N_s = 4$, the Y_v coordinate of the vortex is given by

$$Y_v(\Omega, n, l) = \left(\frac{n}{2} + 2l + 1\right)\frac{\hbar\pi}{md\Omega}, \qquad (18)$$
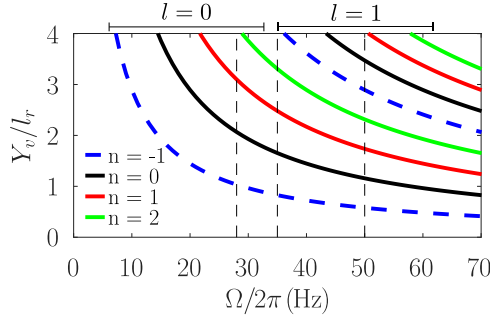
FIG. 3. Vortex coordinate Y_v given by Eq. (18) as a function of rotation frequency Ω. The different types of lines indicate the curves for the possible n values, with $l = 0$ and $l = 1$ for the first and second sequence, respectively. The vertical dashed lines indicate the rotation frequency values $\Omega/2\pi = \{28, 35, 50\}$ Hz.

where $l \geqslant 0$ labels the different sequences of vortices that enter the condensate, for the distinct n values. In Fig. 3 we plot the vortex coordinate Y_v as a function of the rotation frequency, for all n values and the branches with $l = 0$ and $l = 1$. It may be seen that up to $\Omega/2\pi \simeq 35$ Hz only one vortex is nucleated per junction, whereas for increasing Ω a second vortex per junction, with $l = 1$, enters the system for the stationary states with successive n values.

In particular, in Fig. 4 we show the arrays of vortices in the $(x, y, 0)$-plane for the different $n \in \{-1, 0, 1, 2\}$ values at two rotation frequencies, $\Omega/2\pi = 28$ Hz and 50 Hz. The vortex positions of such arrays were extracted from $\psi_n(\mathbf{r})$ of Eq. (1), by means of the plaquette method [34]. The central vortices are related to the imprinted phases necessary to obtain the different $\psi_n(\mathbf{r})$ states. The label $n = 1$ ($n = -1$) corresponds to a singly quantized vortex (antivortex), $n = 2$ to a doubly quantized vortex, and $n = 0$ has no central vortex. Such vortices are present even for low frequencies. In such a figure, one can observe that each, noncentral vortex position is in good agreement with the expression of Y_v which is depicted in Fig. 3, for the different n and l values. For the smaller frequency the vortex positions are accurately reproduced by the $l = 0$ sequence, whereas for the larger frequency, it may be seen, that in Figs. 3(a) and 3(b) a second vortex per junction enters the lattice as expected from Eq. (18) for $l = 1$. By comparing the vortex positions obtained from both approaches one can infer that the estimate derived using the analytic expression for the phases of the LFs is shown to be a very reliable one.

It is interesting to recall that the energy differences between the stationary states $\psi_n(\mathbf{r})$ can change their sign for different frequencies. In particular for $n = \{-1, 0, 1, 2\}$ we have obtained $E_n = \{-4.2, 0, -6.7, -10.8\}10^{-4}\hbar\omega_r + 16.501048\hbar\omega_r$ and $E_n = \{-0.6, 0, 3.9, 3.3\}10^{-4}\hbar\omega_r + 15.213832\hbar\omega_r$, for $\Omega/2\pi = 28$ Hz and $\Omega/2\pi = 50$ Hz, respectively. Hence, for the smaller (larger) frequency the ground state corresponds to $n = 2$ ($n = -1$). By comparing Eq. (15) to Eq. (3), for a given frequency, the stationary states $\psi_n(\mathbf{r})$ have all the same population numbers but differ in the phase differences between neighboring sites $\varphi_k = \phi_{k-1} - \phi_k = -n\pi/2$. Then the small energy differences, around $10^{-4}\hbar\omega_r$, between the states $\psi_n(\mathbf{r})$ can be attributed only to such phase differences.
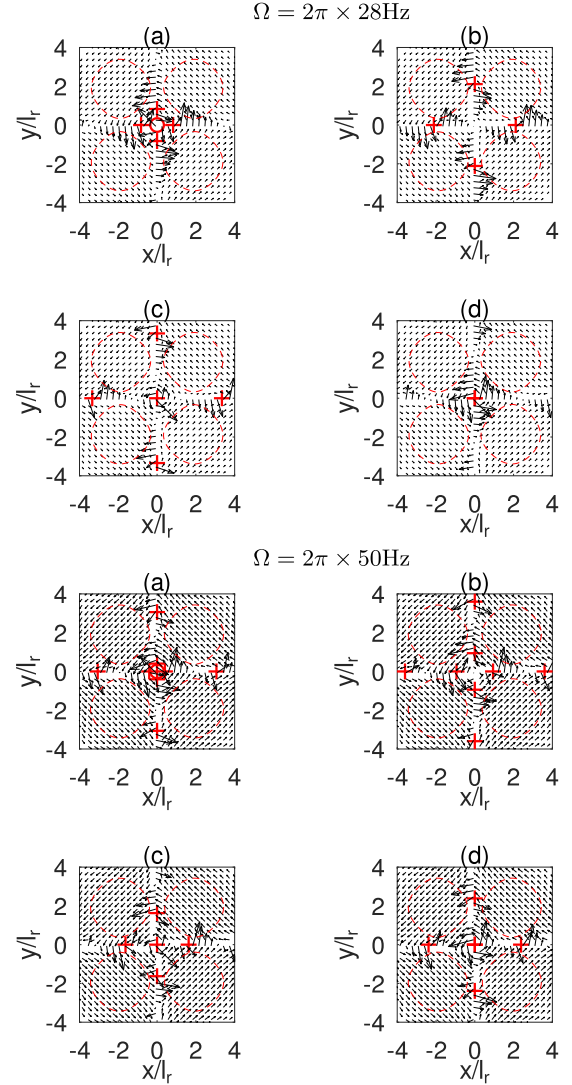

FIG. 4. Stationary vortex arrays at the $z = 0$-plane obtained from $\psi_n(\mathbf{r})$ of Eq. (1), for $\Omega/(2\pi) = 28$ Hz and $\Omega/(2\pi) = 50$ Hz. The black arrows represent the velocity field of the corresponding order parameter. Panels (a) to (d) of each frequency correspond to the different values $n = -1, 0, 1, 2$, respectively. The vortex and antivortex positions, obtained by the plaquette method, are marked with red plus signs and circles, respectively. Note that in the (d) panels, corresponding to $n = 2$, the central plus signs denote doubly quantized vortices centered at $x = y = 0$. The red dashed lines correspond to isodensity curves for a value equal to 5×10^{-3} of the maximum density.

It is important to remark that the previous expression (18) for Y_v does not describe the existence of the central vortices since we have restricted the order parameter to the superposition of only two neighboring LFs, while at the origin the four localized functions should be considered. We thus have

$$\psi_n(0, 0, z) = \frac{1}{\sqrt{N_s}} \sum_k |w_k(0, 0, z)| \, e^{ink2\pi/N_s}, \qquad (19)$$

and since $|w_k(0, 0, z)| = |w_0(0, 0, z)|$, one can ensure the presence of at least one vortex or antivortex along the z axis,

for any $n \neq 0$, given that the previous expression vanishes for such n numbers.

IV. TIME-DEPENDENT NUCLEATION OF VORTICES ON EXTENDED SQUARE LATTICES

We now consider a square lattice with a larger number of sites. We are interested in systems with $N_s > 4$ in order to analyze the effects of the centrifugal force when the system is subject to a time-linear ramp of the rotation frequency. Such a number of sites, which involves different absolute values of the center-of-mass distance to the rotation axis, enables a possible redistribution of particles during the time evolution. We further assume that each site has a high occupation number and that the system forms a bosonic Josephson junction array of N_s weakly linked condensates. In particular, we are interested in studying the appearance of vortices when an initial vortex-free ground state, for $\Omega = 0$, is subject to the linear sweep of the frequency without losing the coherency between neighboring sites during the evolution. Such a type of nucleation process has been experimentally studied in Ref. [24].

We first note that as the system is multiply connected, a single vortex cannot be generated inside the lattice, since the winding number along any closed curve that connects the WLCs through the links cannot be changed spontaneously. As established in the celebrated Helmholtz-Kelvin theorem [35], the winding number around a closed curve is conserved during the time evolution if the superfluid condition is not broken [36]. Therefore, the value of the velocity circulation can change only when a vortex crosses such a curve. Hence, the vortex nucleation process is originated by a vortex that penetrates the system from the outside region, where the superfluid condition is broken. It is worthwhile to mention that another possible process, not observed in our case, could be the creation of a vortex-antivortex pair within the lattice with a later departure of the antivortex.

In this study, we will consider each on-site condensate with the same axial symmetry as has been assumed in the previous sections. Although obtaining complete approximate expressions for the on-site LFs in an arbitrary square lattice does not constitute an easy task [37], we will see that in order to estimate the position of vortices only the phase dependence on the coordinates is needed. Due to this axial symmetry, one can safely assume that the rotation should induce a linear phase with the same analytical expression as that of Eq. (5) on each LF.

On the other hand, taking into account the time-dependent character of the present study, the LFs, the populations, and on-site global phases could evolve in time, and then the order parameter should be approximated by

$$\psi(\mathbf{r}, t) = \frac{1}{\sqrt{N_s}} \sum_{k,p=1}^{\sqrt{N_s}} w_{k,p}(\mathbf{r}, \Omega(t)) \, e^{i\phi_{k,p}(t)} \sqrt{n_{k,p}(t)}, \quad (20)$$

where the indices k and p label the sites in the x and y directions, respectively. We number the sites starting from the corner determined by the smallest and largest, x and y coordinates, respectively. Such indices run from 1 to $\sqrt{N_s}$. The population in each site is given by $N_{k,p} = n_{k,p}N$. In what

follows, for simplicity, we omit writing the Ω dependence on time.

In order to find the vortex position between the $k-1$- and k-sites, for a given p, one can reduce the sum of Eq. (20) to the two nearest-neighboring LFs, and hence $\psi(\mathbf{r}, t)\sqrt{N_s}$ can be approximated by

$$w_{k-1}(\mathbf{r}, \Omega) \, e^{i\phi_{k-1}(t)} \sqrt{n_{k-1}(t)} + w_k(\mathbf{r}, \Omega) \, e^{i\phi_k(t)} \sqrt{n_k(t)}, \quad (21)$$

where for simplicity we have omitted the index p. Approximating the localized function by

$$w_k(\mathbf{r}, \Omega) = |w_k(\mathbf{r}, \Omega)| e^{i\frac{m}{\hbar}(\mathbf{r}-\mathbf{r}_{cm}^k)\cdot(\boldsymbol{\Omega}\times\mathbf{r}_{cm}^k)}, \quad (22)$$

and taking into account that k increases for increasing x values we have $\mathbf{r}_{cm}^k = \mathbf{r}_{cm}^{k-1} + d\hat{x}$, where d is the intersite distance, we may write the phase factor of $w_k(\mathbf{r}, \Omega)$ from Eq. (22) as

$$(\mathbf{r} - \mathbf{r}_{cm}^k) \cdot (\boldsymbol{\Omega} \times \mathbf{r}_{cm}^k) = (\mathbf{r} - \mathbf{r}_{cm}^{k-1}) \cdot (\boldsymbol{\Omega} \times \mathbf{r}_{cm}^{k-1}) + y\Omega d. \quad (23)$$

By introducing (22) and (23) in Eq. (21) one obtains the following condition for the vortex position $\mathbf{R}_v^{(k)} = (X_v^{(k)}, Y_v^{(k)}, z)$:

$$\sqrt{n_k(t)} |w_k(\mathbf{R}_v^{(k)}, \Omega)| \, e^{i(\frac{m\Omega d}{\hbar}Y_v^{(k)} - \varphi_k(t))}$$
$$+ \sqrt{n_{k-1}(t)} |w_{k-1}(\mathbf{R}_v^{(k)}, \Omega)| = 0, \quad (24)$$

where $\varphi_k(t) = \phi_{k-1}(t) - \phi_k(t)$ is the phase difference between such neighboring sites, with $-\pi < \varphi_k(t) < \pi$. The superscript (k) in the vortex position denotes that it belongs to the path parallel to the y axis that separates the sites labeled with $k-1$ and k. Then, from the imaginary part of Eq. (24), one can derive the expression for the vortex coordinate,

$$Y_v^{(k)}(t) = \left(\frac{\varphi_k(t)}{\pi} + 2l_k + 1 \right) \frac{\pi\hbar}{md\Omega}, \quad (25)$$

where l_k is an integer number that labels the vortices located along such a path parallel to the y axis. If one wants to calculate $Y_v^{(k)}(t)$ along the whole low-density straight line that crosses the lattice, one should incorporate in Eq. (25) the phase differences $\varphi_k(t)$ for all the p values. However, due to the fourfold symmetry of the square lattice one can restrict the study to $Y_v^{(k)} > 0$, which is given for $p \leqslant \sqrt{N_s}/2$ and $l_k \geqslant 0$.

Finally, we note that, from the real part of Eq. (24) one should obtain the transversal coordinate $X_v^{(k)}(t)$ of the vortex along such a straight path, if having at hand $|w_k(\mathbf{R}_v^{(k)}, \Omega)|$, which is not the present case. Although possible variations on the site populations, N_k and N_{k-1}, could lead to slight shifts in such transversal coordinate, this effect turns out to be almost imperceptible due to the tight on-site localization, as we have observed from our numerical GP simulations. Then we will consider such x values constant along the straight lines parallel to the y axis.

In the following subsection we will show the usefulness of the previous formula for determining the number of nucleated vortices.

A. Number of nucleated vortices

In what follows, we will be focused on the number of vortices that become nucleated on the lattice as a function of Ω, which turns to be an increasing function of time. Assuming the vortices are generated outside the lattice, one can obtain

such a number by counting how many vortices enter into the low-density paths by what we will call entrances. Taking into account the fourfold symmetry, we will consider only the $Y_v^{(k)} > 0$ case. Being the first vortex labeled by $l_k = 0$, the number of vortices, for a given Ω, that enter by such an entrance reads $N_v^{(k)} = l_k^{(L)} + 1$, with $l_k^{(L)}$ the largest l_k value. The value of $l_k^{(L)}$ as a function of Ω can be obtained through Eq. (25) with the condition that $Y_v^{(k)}$ is located at the entrance, hence $Y_v^{(k)} = d\sqrt{N_s}/2$, where $\sqrt{N_s}/2$ is the number of sites in the y direction (labeled by p), up to the x axis. Then, replacing $N_v^{(k)} = l_k^{(L)} + 1$, we finally obtain

$$N_v^{(k)}(t) = \left\| \frac{md^2\sqrt{N_s}\Omega}{4\pi\hbar} - \frac{\varphi_k(t)}{2\pi} + \frac{1}{2} \right\|. \quad (26)$$

Given that the time evolution depends on the way the rotation frequency is varied, we can obtain only bounds of the previous expression taking into account $-\pi < \varphi_k(t) < \pi$, which yield

$$N_-^{(k)} = \left\| \frac{md^2\sqrt{N_s}\Omega}{4\pi\hbar} \right\| \quad (27)$$

and

$$N_+^{(k)} = \left\| \frac{md^2\sqrt{N_s}\Omega}{4\pi\hbar} \right\| + 1, \quad (28)$$

for the lower and upper bounds, respectively.

Multiplying by the number of entrances around the lattice $4(\sqrt{N_s} - 1)$, and approximating the integer part function by a straight line that passes by the middle points of the steps, we obtain $\|X\| \simeq X - 1/2$, for $X > 0$, we conclude that the total number of vortices N_v inside the lattice lies between the following values:

$$N_v^{(\pm)} = 4(\sqrt{N_s} - 1)\left(\frac{md^2\sqrt{N_s}\Omega}{4\pi\hbar} \right) \pm 2(\sqrt{N_s} - 1), \quad (29)$$

which can be rewritten as

$$N_v^{(\pm)} = \frac{md^2(N_s - \sqrt{N_s})\Omega}{\hbar\pi} \pm 2(\sqrt{N_s} - 1). \quad (30)$$

Finally, an estimate of such a number of nucleated vortices can be obtained as the average of $N_v^{(\pm)}$ which yields

$$N_v = \frac{md^2(N_s - \sqrt{N_s})\Omega}{\hbar\pi}. \quad (31)$$

Consequently, the total number of vortices nucleated in the lattice is a linear function of Ω in agreement with the experimental observation of [24]. We note that Eq. (31) differs from the best estimate used in [24], where it is assumed that the density of vortices for a given Ω, whether a lattice is present or not, is $n_v = m\Omega/\pi\hbar$. Then the total number of vortices follows the Feynman's rule [38] $N_v^F = m\Omega R^2/\hbar$, where R is the Thomas-Fermi radius. In Ref. [24] the authors claim that, when working with WLCs, a good estimate for their results is given by a straight line which is obtained by using a fixed $R(\Omega) = R(\Omega = 0)$, instead of considering an increasing $R(\Omega)$. Such an approximation in terms of the number of sites N_s and the intersite distance d may be rewritten as $N_v^F = m\Omega d^2 N_s/\pi\hbar$, given that the area πR^2 should be replaced by $N_s d^2$. Here, by assuming that the vortices are coming from
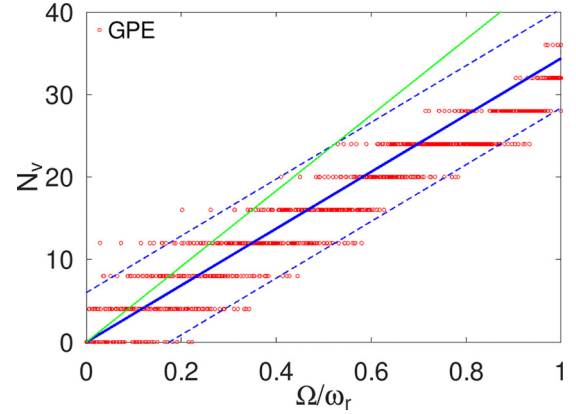

FIG. 5. Number of vortices N_v as a function of the rotation frequency Ω for $V_b = 75\hbar\omega_r$. The red points correspond to time-dependent GP simulations, obtained by solving Eq. (32), whereas the blue lines indicate our predictions; in particular, the solid line indicates the mean value given by Eq. (31), and the dashed lines correspond to the upper and lower bounds from Eq. (30). The green solid line, with the higher slope, corresponds to the estimate $N_v^F = m\Omega d^2 N_s/\pi\hbar$.

outside the lattice, we have obtained a smaller slope due to the subtraction of the term $\sqrt{N_s}$ inside the parentheses of Eq. (31).

The numerical simulations are performed by solving the 3D time-dependent GP equation,

$$i\hbar \frac{\partial}{\partial t} \psi_{\text{GP}}(\mathbf{r}, t) = [\hat{H}_0 + gN|\psi_{\text{GP}}(\mathbf{r}, t)|^2 - \boldsymbol{\Omega}(t) \cdot \hat{L}]\psi_{\text{GP}}(\mathbf{r}, t), \quad (32)$$

using as the initial order parameter, $\psi_{\text{GP}}(\mathbf{r}, 0)$, the ground state of the nonrotating system. The rotation angular frequency $\boldsymbol{\Omega}(t) = \Omega(t)\hat{z}$ is linearly increased in time from zero up to $\omega_r\hat{z}$, with a ramping time interval $\tau = 10^3/\omega_r$. We change the lattice intersite distance to $d = 3l_r$ to simplify the notation, and use a less confining harmonic potential with $\omega_r = 2\pi \times 10$ Hz and $\omega_z = 2\pi \times 20$ Hz. The number of sites is increased to $N_s = 16$ and the total number of particles to $N = 4 \times 10^4$. In Figs. 5 and 6 we show the number of vortices nucleated within a lattice as a function of Ω, for $V_b = 75\hbar\omega_r$ and $V_b = 40\hbar\omega_r$, respectively. For both barriers the system is formed by WLCs, being the barriers 1.3 to 1.9 larger than the chemical potential of the ground state. In order to observe how the results are affected when the fourfold symmetry is slightly broken, a fact that can also occur in an experiment, we discuss two possibilities shown in Fig. 6. In the upper panel we present the results when a small perturbation in the initial populations of the ground state has been applied, and in the bottom one, we perform a slight displacement $\delta\mathbf{r} = 0.1l_r(\hat{x} + \hat{y})$ of the axis of the harmonic potential. One can observe that a number of nucleated vortices different from a multiple of four is now allowed, and hence a smaller spreading of the points with respect to the line that estimates the mean value is attained. In each case we also draw the estimate $N_v^F = m\Omega d^2 N_s/\pi\hbar$, which corresponds to $N_v^F = m\Omega R(\Omega = 0)^2/\hbar$ given in Ref. [24]. We note that, when drawing the points of Figs. 5 and 6, we count the total number of GP vortices by adding the vortices and subtracting the antivortices, both obtained by the plaquette
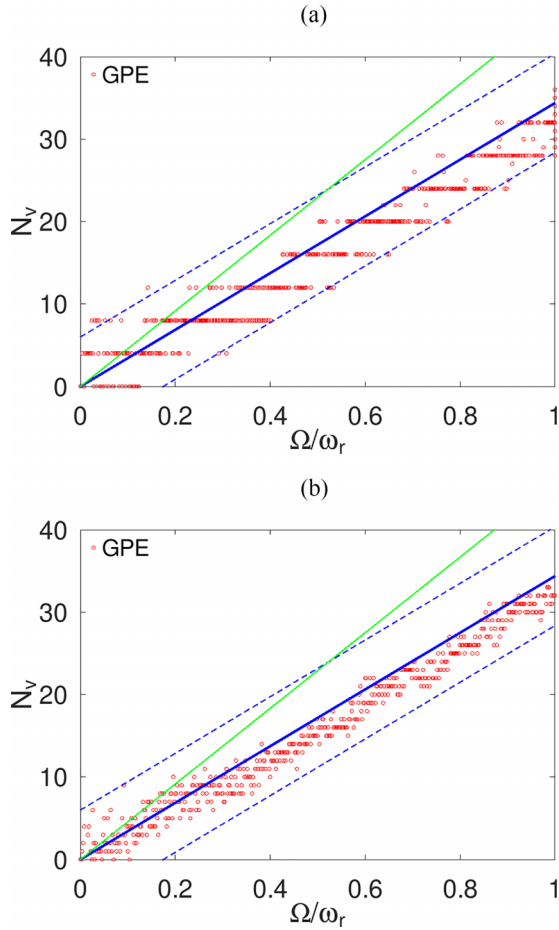
FIG. 6. Number of vortices N_v as functions of the rotation frequency Ω for $V_b = 40\hbar\omega_r$. The points correspond to time-dependent GP results from Eq. (32). The top panel (a) corresponds to simulations using small perturbed initial populations, and the points in the bottom panel (b) were obtained using a slightly shifted harmonic potential, $\frac{1}{2}m[\omega_r^2(x - 0.1l_r)^2 + \omega_r^2(y - 0.1l_r)^2 + \omega_z^2 z^2]$. The lines are the same as in Fig. 5.

method, up to the borders of the lattice. However, at such borders, some fluctuations appear which give rise to the points that exceed the upper and lower bounds.

From our numerical calculation it may be seen that, for the present dynamical vortex nucleation process, Feynman's rule can be improved when applied to an optical lattice. Moreover, although our approximation has been derived for a different system, it is easy to verify that it better describes the experimental data for the higher barrier of Ref. [24], which correspond to WLCs.

In the next section we will see that the outer sites do not increase their populations as expected from the centrifugal distortion, and hence support the fact of working with a fixed number of sites during the whole dynamics. It is important to distinguish our dynamical nucleation process from the theoretical study [25] where the dissipative parameter allows the system to relax into a wider lattice and hence the number of nucleated vortices increases faster with Ω. Another difference is the critical rotation frequency $\Omega_c/\omega_r \simeq 0.2$ needed in Ref. [25] to start nucleating vortices.

In Figs. 5 and 6 one can observe that the number of nucleated vortices exhibits fast variations as a function of the rotation frequency. Such rapid variations are related to the fact that a self-trapping (ST) dynamics, with very short time periods, is triggered, which in turn provokes a rapid movement of vortices. In the following subsection we will analyze such a vortex dynamics.

B. Vortex dynamics

In a homogeneous BEC, the vortex velocity is determined by the background superfluid velocity through the Magnus force [1,39,40], whereas in a nonhomogeneous BEC, the vortex velocity acquires an additional term which depends on the density gradient [17,40–42] and on the form of the vortex core [42]. In systems where the order parameter can be written in terms of LFs, an instantaneous passage of a vortex can be easily predicted. However, in these cases, no relation between the velocity of the vortex and the macroscopic coordinates, of the type of Eq. (25), has been established. In particular, in nonrotating double-well systems, such passage of vortices across the junctions has been related to the presence of phase slips [43] which occurs in the ST regime [44,45]. Their motion turns to be much faster than the variation of the macroscopic coordinates which describe the relevant dynamics. We recall that the ST regime is characterized by a phase difference time derivative that never vanishes and is referred to as running phase [44,45]. It is worthwhile noting that the ST behavior is also encountered in lattice systems [33,46], showing the same phase difference behavior. In this section we will show that in rotating systems the GP vortex dynamics is in close connection with the evolution of the phase difference between neighboring sites, as stated in Eq. (25), and hence they share the same time periods.

In stationary conditions, attained from a GP energy minimization procedure, each phase difference and population should remain static. However, the static population in each site should differ for distinct constant frequencies due to the centrifugal force. Here we may distinguish three sets of sites according to their center-of-mass distance to the rotation axis, namely, the central (C), lateral (L), and diagonal (D) ones, consisting of four, eight, and four sites, respectively (see inset of Fig. 7). In the notation of Eq. (20), the central site labels k and p are given by the combinations of the numbers {2, 3}, the diagonal by {1, 4}, and the lateral by the rest ones. Hence, the centrifugal force should push particles from central to lateral sites, and from lateral to diagonal ones as marked with arrows in the right corner of inset of Fig. 7. In the top panel of Fig. 7, we show as dashed lines the number of particles in the different types of sites in stationary conditions as a function of the static rotation frequency. It may be seen, for example, that all sites acquire the same number of particles when $\Omega = \omega_r$, due to the full compensation of the harmonic trapping with the centrifugal force.

For the barrier of Fig. 5, we found that the number of particles in each site remains fixed at their initial value during all the time evolution, whereas, for the lower barrier, a different evolution of the populations is encountered. In Fig. 7 we show the low barrier height case with $V_b = 40\hbar\omega_r$, which is nearer to the chemical potential which is about $\mu \simeq 30\hbar\omega_r$. It may
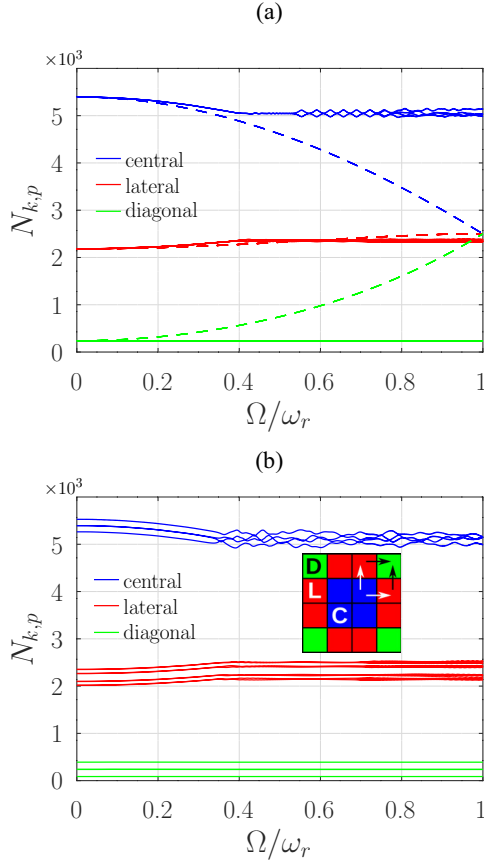
FIG. 7. Site populations $N_{k,p}$ as functions of Ω, which are depicted with solid lines, were obtained by solving Eq. (32) during the time sweep of the frequency, for $V_b = 40\hbar\omega_r$. The top (a) and bottom (b) panels correspond to the same cases of Fig. 6. The blue (upper) lines, the red (middle) lines, and the green (lower) lines correspond to the number of particles in the central, lateral, and diagonal sites, respectively. The correspondence between the indices k, p and the different sets of sites is explained in the text. The dashed lines in the top panel depict the GP stationary populations at the corresponding static frequency, obtained via a minimization procedure.

be seen that there exists an initial movement of particles to the more external sites up to $\Omega \simeq 0.4\omega_r$. In particular, in that range of frequencies, a sizable number of particles move from the central sites to the lateral ones. For larger values of Ω, the populations perform only small oscillations around some fixed numbers.

In what follows we will see how the populations $N_{k,p}$, the phase differences, and the vortices evolutions are related when the time-linear ramp of the rotation frequency is applied. As a consequence of the phase differences evolution a dynamics of vortices appears as expected from Eq. (25), which exhibits distinct behaviors. More precisely, for neighboring sites that belong to the same set (C, L, or D), very small variations of the phase differences are observed, and hence, the vortices located between such sites move slowly, whereas, when the neighboring sites belong to different sets, and the populations turn to be far from the stationary configuration values, running phase differences, with related fast vortex dynamics, develop. Hence, the fast variation of the phase differences, connected to
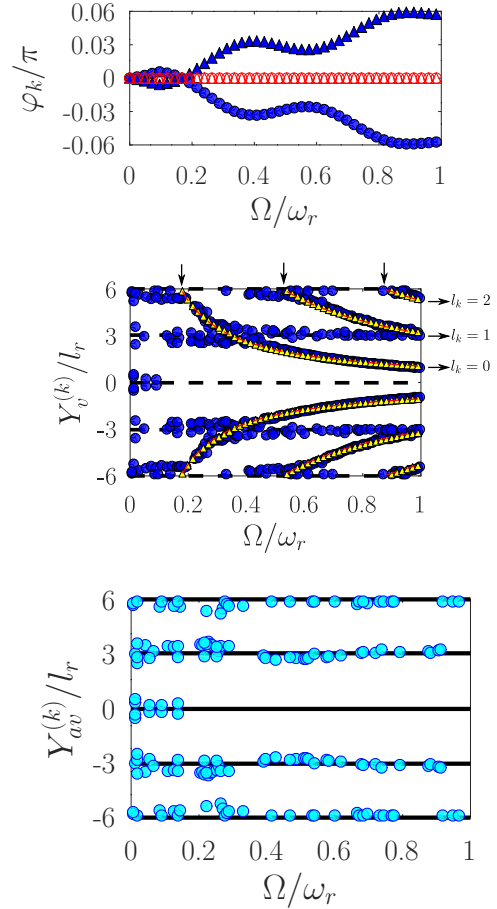

FIG. 8. Top panel: GP phase differences between sites at both sides along $x = 0$, $\varphi_{k,p} = \phi_{k-1,p} - \phi_{k,p}$, which are given for $k = 3$ and $p = 1$ to 4, as functions of Ω, for $V_b = 75\hbar\omega_r$. The phase difference between the lateral sites for $y > 0$ ($y < 0$) with $p = 1$ ($p = 4$) is depicted with blue filled triangles (circles), whereas the difference between the central sites for $y > 0$ ($y < 0$) with $p = 2$ ($p = 3$) is depicted with red hollow triangles (circles). Middle panel: Vortex positions along the $x = 0$ low-density path. The positions extracted from the order parameter of Eq. (32), obtained by the plaquette method, are depicted with blue dots, whereas the red dashed line and the yellow triangles, almost superimposed on the blue dots, correspond to Eq. (25) replacing $\varphi_k(t)$ by zero and by the GP $\varphi_{3,p}(t)$ of the top panel, respectively. Bottom panel: Antivortices obtained through GP simulations.

a ST regime, seems to be the responsible for the permanence of almost all the particles within the same sites of the nonrotating system. Such an observation of the atoms remaining within the initial confinement has also been reported in the experimental work [24].

We first study the dynamical nucleation process along the low-density paths that separate sites belonging to the same set, such as the $x = 0$ path, where the phase differences are calculated between two central sites and two lateral ones. In the notation of Eq. (20) such phase differences are given by $\varphi_{3,p}(t) = \phi_{2,p}(t) - \phi_{3,p}(t)$ with $p = 1$ to 4. From the top panel of Fig. 8 it may be seen that the phase differences remain almost vanishing, since $|\varphi_k(t)|/\pi \leqslant 0.06$, and thus a reasonable estimate for the position of vortices can be obtained

using Eq. (25) with $\varphi_k = 0$, for all p values. In the middle panel of Fig. 8 we display the vortex positions. Focusing on the vortices with $Y_v^{(k)} > 0$, with $k = 3$, we may see that the positions obtained from Eq. (25) with φ_k replaced by the GP results $\varphi_{k,p}(t)$ (for $k = 3$ and $p = 1, 2$ values) and with $\varphi_k = 0$, where we have used $l_k = 0, 1$, and 2, are superposed, and hence the variation of the phase differences has no sizable effect on the vortex nucleation at the axes. Moreover, both curves are in good accordance with the points extracted from the time-dependent GP simulations using the plaquette method. We note that at the end of the evolution there are three vortices located at the points marked with horizontal arrows in the middle panel that have entered the lattice at the frequencies indicated with vertical arrows. Given that the largest l_k value is $l_k^{(L)} = 2$ the number of vortices that entered through the top entrance is in fact $N_v^{(k)} = l_k^{(L)} + 1 = 3$, as stated above Eq. (26). The reflection symmetry observed in such a panel is a direct consequence of the fourfold symmetry of the lattice. Then, by the four entrances located at the axes, during the whole evolution 12 vortices penetrate in the system.

It is important to mention that many vortex-antivortex pairs are created and annihilated instantaneously throughout the GP dynamics, especially near the intersections of the low-density paths. Hence, as we are depicting only the vortices, in the middle panel, some points that appear occasionally in the graph correspond to such vortex-antivortex fluctuations, and they do not contribute to the net number of nucleated vortices, as they cancel each other. In the bottom panel of Fig. 8 we show the antivortices positions. Such antivortices appear, as we have stated around the intersections of the paths, where the approximation of Eq. (25) is not appropriate for predicting the existence of vortices, since the four LFs should be taken into account. We want to mention that by analyzing the three-dimensional structure of such vortex-antivortex pairs, we have observed that they do not correspond to straight vortex lines, and in some cases they form part of a vortex ring.

For the paths that separate neighboring sites belonging to different sets (C, L, or D), the time-dependent nucleation of vortices is not only due to the process observed at the axes. The phase differences time variations, between the centers of such sites, can also provoke the penetration and departure of vortices, and hence change the values of $l_k^{(L)}$. In particular, when the on-site populations depart sizably from their stationary values, the vortex nucleation process is combined with a rapid motion of vortices. The fast vortex dynamics seems to be related to the fact that the macroscopic coordinates enter a self-trapping regime characterized by an almost constant occupation number and a running phase difference between such neighboring sites. From Eq. (25) one can infer that an increasing (decreasing) running phase should produce a monotonous increasing (decreasing) vortex coordinate. In our system such dynamics develops along the four low-density paths defined by the straight lines $x = \pm 3l_r$ and $y = \pm 3l_r$, which separate sites of distinct sets. In Fig. 9 we illustrate such behavior along the path located at $x = -3l_r$, when the linear ramp has been switched off, and hence around six vortices have been nucleated. In the top panel we show the phase differences $\varphi_{k,p}(t) = \phi_{k-1,p}(t) - \phi_{k,p}(t)$ for $k = 2$ and different $1 \leqslant p \leqslant 4$ values, from time-dependent GP simulations. In the bottom panel we
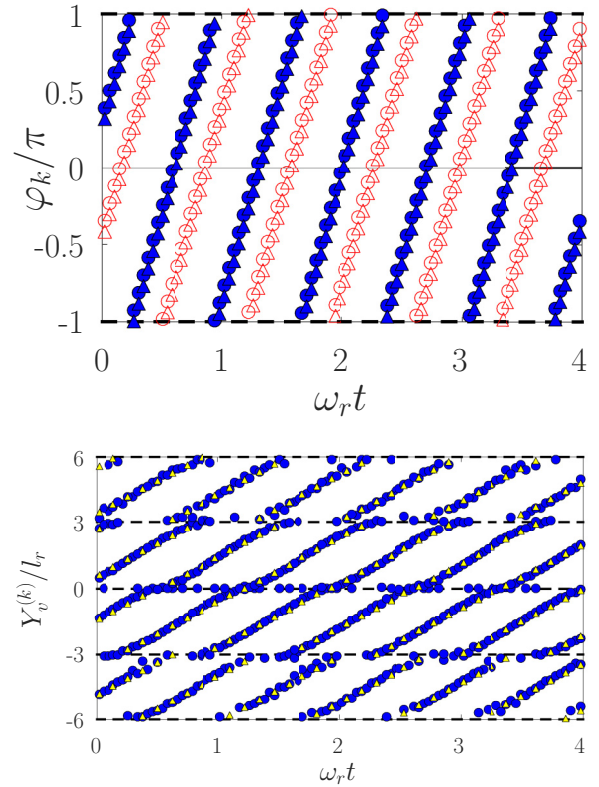

FIG. 9. Top panel: The phase differences as function of time between both sides of the line $x/l_r = -3$, $\varphi_{k,p}(t) = \phi_{k-1,p}(t) - \phi_{k,p}(t)$, for $k = 2$ and $p = 1 - 4$. The phase difference between the diagonal and lateral sites $\varphi_{2,1}(\varphi_{2,3})$, for $y > 0$ ($y < 0$) is depicted with blue filled triangles (circles), whereas the difference between the lateral and central sites for $y > 0$ ($y < 0$) with index $p = 2$ ($p = 3$) is depicted with red hollow triangles (circles). Given the high symmetry of the system both curves with blue (red) points are superimposed. Bottom panel: The vortex positions $Y_v^{(k)}$ as function of time are depicted with blue dots for time-dependent GP simulations by solving Eq. (32), and the yellow triangles (almost on top of the blue ones) are obtained through Eq. (25) replacing $\varphi_2(t)$ by the GP results $\varphi_{2,p}(t)$, with $p = 1$ to $p = 4$, which yield the different $Y_v^{(2)}$ values from top to bottom. The barrier height is $V_b = 75\hbar\omega_r$, and the time interval has been extracted after the linear ramp was switched off.

show the vortex coordinate extracted from time-dependent GP simulations, through the plaquette method. Almost on top of such points, indicated with yellow triangles, one can view the points estimated by Eq. (25) using the time-dependent GP-phase differences, showing the very good agreement between both approaches. Hence, one can conclude that such vortex dynamics is ruled by the phase differences evolution, rather than by density gradients which become useful in other types of systems. Furthermore, such vortex dynamics is much more rapid than the typical timescales involved in the whole process provided by the linear ramp. In the bottom panel it may be seen that vortices enter the lattice from the bottom entrance and depart from the top one at different times, which explains the rapid variation of the nucleated vortices inside the lattice. It is worthwhile recalling that if the fourfold symmetry is broken, as in the case of the bottom panel of Fig. 6, the fluctuation on the total number of vortices has shown to exhibit a
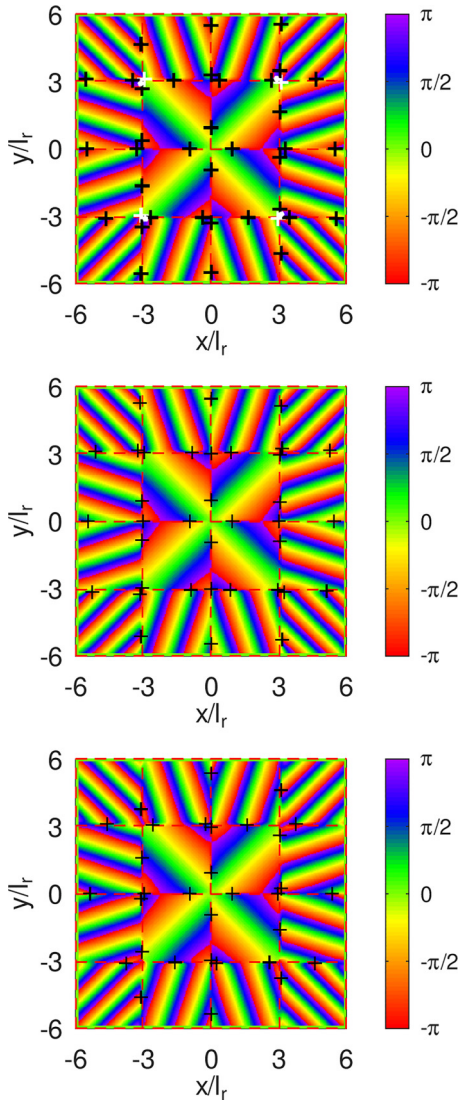
FIG. 10. The phase of the GP order parameter, obtained by solving Eq. (32), is depicted in colors at the $z = 0$ plane. The corresponding vortex locations, obtained by the plaquette method, are marked with plus signs, whereas the antivortices with circles. The nucleated vortices are marked with black symbols, whereas vortex-antivortex pairs, in the top panel around $|x| = |y| = 3l_r$, are depicted with white symbols. The barrier height corresponds to $V_b = 75\hbar\omega_r$. The three times were selected at the end of the ramp, at $\omega_r t = 999.8$ (top panel), 1000.0 (middle panel), and 1000.2 (bottom panel). In each panel the color scale corresponds to $\arg(\psi_{GP}(\mathbf{r}, t))$ at the selected time.

smaller amplitude. A plausible explanation of such an effect could be that the vortices that move along the four straight lines $x = \pm 3l_r$ and $y = \pm 3l_r$, do not enter, or exit, the system simultaneously.

Finally, to better visualize the vortex dynamics in Fig. 10 we mark with plus signs the positions of vortices obtained by time-dependent GP simulations, in the $z = 0$ plane, at three times around $t \simeq 1000\omega_r^{-1}$. In such figure, we also show in colors the phase of the GP order parameter where one can first view that the phases are, in fact, linear on such coordinates at each site, as we have assumed, and that the phase gradient

increases with an increasing center-of-mass distance to the rotation axis. In other words, the central, lateral, and diagonal sites have increasing phase gradients in such an order. Second, the vortices are clearly located along the six paths defined by the straight lines, $x/l_r = -3, 0, 3$ and $y/l_r = -3, 0, 3$. Along the axes $x = 0$ and $y = 0$ the vortices perform only very small oscillations, and hence their total number remains fixed at six vortices per axis in the time interval considered, and the positions are in agreement with those nucleated at the end of the evolution of Fig. 8, which are marked with horizontal arrows at the middle panel of such a figure. On the other hand, for the other four straight lines $x/l_r = \pm 3$ or $y/l_r = \pm 3$, the running phase difference, shown in Fig. 9, generates a vortex dynamics, which can involve either the ingress or the exit of vortices from the lattice. For example, at $x = -3l_r$ it may be seen, by following the movement of the vortex which is around $y = 5l_r$ at the top panel of Fig. 10, that it moves in the positive y direction to its position in the middle panel, and finally it disappears at the bottom panel. Hence, one has six vortices moving in such direction, except in the lower panel where only five remain. Once more, such dynamics explains the change, from 36 to 32, of the total number of vortices nucleated, in such a short time interval. Using our estimate of Eq. (31), the number of vortices yields 34.4 in contrast to Feynman's rule applied to our 16-site system, which reads 45.8. The top panel also illustrates the appearance of vortex-antivortex pairs, around the points that satisfy $|x| = |y| = 3l_r$, that disappear in the middle panel. We note that such fluctuations are concentrated in the lower density regions.

V. CONCLUSIONS

For a four-site system which forms a ring lattice, by using an accurate expression for the phases of the on-site localized functions, we have analytically obtained the arrays of vortices for the four different stationary states with a given rotation frequency. By comparing with the GP results, we have shown that our analytical estimates for such vortex positions turn out to be very accurate.

Hence, in a second step, making use of the same type of expressions, we have investigated a vortex nucleation process for a square lattice with a larger number of sites. Such a process consists on applying a a time-linear ramp of the rotation frequency, similar to the method used in the experiment of Ref. [24]. By analyzing such a dynamical process, we found that the on-site populations perform small oscillations around numbers very close to the initial ones, and that the phase differences between different types of sites exhibit a running phase behavior as function of time, typical of a ST regime. As a consequence of such a behavior, the expanding effect of the centrifugal force was canceled. An analogous observation, for WLCs, has been reported in Ref. [24], where the experimental results do not reflect an increasing Thomas-Fermi confinement radius as expected from a centrifugal distortion.

With respect to the number of nucleated vortices we have obtained a linear dependence on the rotation frequency similar to the estimate $N_v^F = m\Omega d^2 N_s / \pi\hbar$ used in Ref. [24] for WLCs. However, our prediction differs from such an estimate, given that, instead of being proportional to the number of involved sites, it turns to be proportional to $N_s - \sqrt{N_s}$. By

introducing the parameters of the experiment of Ref. [24] in our formula, it seems to better reproduce their experimental results. Although our approach was derived for a specific system, we believe that the new factor which is related to the number of entrances should also be present in the vortex nucleation estimates of other types of lattice potentials.

Finally, the nucleation of vortices in other systems of current interest such as a rotating supersolid dipolar gas [26,27] with regular patterns in the density could be suitable for applying the present approach. Given that each droplet exhibits an almost axial symmetry around an axis parallel to the rotation axis, when subject to rotation its velocity field can be approximated by an homogenous one [30]. Then the rotation-induced phase on the droplet should have a linear dependence on the

coordinates, which constitutes the main requirement for the application of the present treatment. Since rotation may compromise the density pattern of the nonrotating ground state [27,47], the study should contemplate the possible changes, when varying the rotation frequency, in the number of droplets and their distribution.

[1] R. J. Donnelly, *Quantized Vortices in Helium II* (Cambridge University Press, Cambridge, 1991).

[2] F. Dalfovo, S. Giorgini, L. P. Pitaevskii, and S. Stringari, Rev. Mod. Phys. **71**, 463 (1999).

[3] M. R. Matthews, B. P. Anderson, P. C. Haljan, D. S. Hall, C. E. Wieman, and E. A. Cornell, Phys. Rev. Lett. **83**, 2498 (1999).

[4] B. P. Anderson, P. C. Haljan, C. E. Wieman, and E. A. Cornell, Phys. Rev. Lett. **85**, 2857 (2000).

[5] A. L. Fetter, Rev. Mod. Phys. **81**, 647 (2009).

[6] K. W. Madison, F. Chevy, W. Wohlleben, and J. Dalibard, Phys. Rev. Lett. **84**, 806 (2000).

[7] J. Abo-Shaeer, C. Raman, J. Vogels, and W. Ketterle, Science **292**, 476 (2001).

[8] P. Engels, I. Coddington, P. C. Haljan, V. Schweikhard, and E. A. Cornell, Phys. Rev. Lett. **90**, 170405 (2003).

[9] V. Bretin, S. Stock, Y. Seurin, and J. Dalibard, Phys. Rev. Lett. **92**, 050403 (2004).

[10] S. Stock, B. Battelier, V. Bretin, Z. Hadzibabic, and J. Dalibard, Laser Phys. Lett. **2**, 275 (2005)

[11] C. Ryu, M. F. Andersen, P. Cladé, V. Natarajan, K. Helmerson, and W. D. Phillips, Phys. Rev. Lett. **99**, 260401 (2007).

[12] S. Eckel, J. G. Lee, F. Jendrzejewski, N. Murray, C. W. Clark, C. J. Lobb, W. D. Phillips, M. Edwards, and G. K. Campbell, Nature (London) **506**, 200 (2014).

[13] K. E. Wilson, E. C. Samson, Z. L. Newman, and B. P. Anderson, Phys. Rev. A **106**, 033319 (2022).

[14] A. L. Fetter, B. Jackson, and S. Stringari, Phys. Rev. A **71**, 013605 (2005).

[15] J. K. Kim and A. L. Fetter, Phys. Rev. A **72**, 023619 (2005).

[16] P. Capuzzi and D. M. Jezek, J. Phys. B: At. Mol. Opt. Phys. **42**, 145301 (2009).

[17] D. M. Jezek, P. Capuzzi, M. Guilleumas, and R. Mayol, Phys. Rev. A **78**, 053616 (2008).

[18] J. W. Reijnders and R. A. Duine, Phys. Rev. Lett. **93**, 060401 (2004).

[19] J. W. Reijnders and R. A. Duine, Phys. Rev. A **71**, 063607 (2005).

[20] H. Pu, L. O. Baksmaty, S. Yi, and N. P. Bigelow, Phys. Rev. Lett. **94**, 190401 (2005).

[21] S. Tung, V. Schweikhard, and E. A. Cornell, Phys. Rev. Lett. **97**, 240402 (2006).

[22] R. K. Kumar, L. Tomio, and A. Gammal, J. Phys. B: At. Mol. Opt. Phys. **52**, 025302 (2019).

[23] A. S. Hassan, A. M. Elbadry, A. A. Mahmoud, A. M. Mohammedein, and A. M. Abdallah, J. Low Temp. Phys. **200**, 102 (2020).

[24] R. A. Williams, S. Al-Assam, and C. J. Foot, Phys. Rev. Lett. **104**, 050404 (2010).

[25] A. Kato, Y. Nakano, K. Kasamatsu, and T. Matsui, Phys. Rev. A **84**, 053623 (2011).

[26] S. M. Roccuzzo, A. Gallemí, A. Recati, and S. Stringari, Phys. Rev. Lett. **124**, 045702 (2020).

[27] A. Gallemí, S. M. Roccuzzo, S. Stringari, and A. Recati, Phys. Rev. A **102**, 023322 (2020).

[28] F. Ancilotto, M. Barranco, M. Pi, and L. Reatto, Phys. Rev. A **103**, 033314 (2021).

[29] L. Klaus, T. Bland, E. Poli, C. Politi, G. Lamporesi, E. Casotti, R.l N. Bisset, M. J. Mark, and F. Ferlaino, Nat. Phys. **18**, 1453 (2022).

[30] M. Nigro, P. Capuzzi, and D. M. Jezek, J. Phys. B: At. Mol. Opt. Phys. **53**, 025301 (2020).

[31] E. P. Gross, Nuovo Cimento **20**, 454 (1961); L. P. Pitaevskii, Zh. Eksp. Teor. Fiz. **40**, 646 (1961) [Sov. Phys. JETP **13**, 451 (1961)].

[32] H. M. Cataldo and D. M. Jezek, Phys. Rev. A **84**, 013602 (2011).

[33] M. Nigro, P. Capuzzi, H. M. Cataldo, and D. M. Jezek, Phys. Rev. A **97**, 013626 (2018).

[34] C. J. Foster, P. B. Blakie, and M. J. Davis, Phys. Rev. A **81**, 023623 (2010).

[35] L. D. Landau and E. M. Lifshitz, *Fluid Mechanics* (Butterworth-Heinemann, New York, 1995).

[36] B. Damski and K. Sacha, J. Phys. A: Math. Gen. **36**, 2339 (2003).

[37] K. Kasamatsu, Phys. Rev. A **79**, 021604(R) (2009).

[38] R. P. Feynman, Prog. Low Temp. Phys. A **1**, 17 (1955).

[39] V. Ambegaokar, B. I. Halperin, David R. Nelson, and Eric D. Siggia, Phys. Rev. B **21**, 1806 (1980).

[40] D. E. Sheehy and L. Radzihovsky, Phys. Rev. A **70**, 063620 (2004).

[41] H. M. Nilsen, G. Baym, and C. J. Pethick, Proc. Natl. Acad. Sci. USA **103**, 7978 (2006).

[42] D. M. Jezek and H. M. Cataldo, Phys. Rev. A **77**, 043602 (2008).

[43] M. Abad, M. Guilleumas, R. Mayol, F. Piazza, D. M. Jezek, and A. Smerzi, Europhys. Lett. **109**, 40005 (2015).

[44] A. Smerzi, S. Fantoni, S. Giovanazzi, and S. R. Shenoy, Phys. Rev. Lett. **79**, 4950 (1997).

[45] S. Raghavan, A. Smerzi, S. Fantoni, and S. R. Shenoy, Phys. Rev. A **59**, 620 (1999).

[46] C. E. Creffield, Phys. Rev. A **75**, 031607(R) (2007); J.-K. Xue, A.-X. Zhang, and J. Liu, *ibid.* **77**, 013602 (2008); T. J. Alexander, E. A. Ostrovskaya, and Y. S. Kivshar, Phys. Rev. Lett. **96**, 040401 (2006); B. Liu, L.-B. Fu, S.-P. Yang, and J. Liu, Phys. Rev. A **75**, 033601 (2007); Th. Anker, M. Albiez, R. Gati, S. Hunsmann, B. Eiermann, A. Trombettoni, and M. K. Oberthaler, Phys. Rev. Lett. **94**, 020403 (2005); B. Wang, P. Fu, J. Liu, and B. Wu, Phys. Rev. A **74**, 063610 (2006).

[47] A. Gallemí and L. Santos, Phys. Rev. A **106**, 063301 (2022).